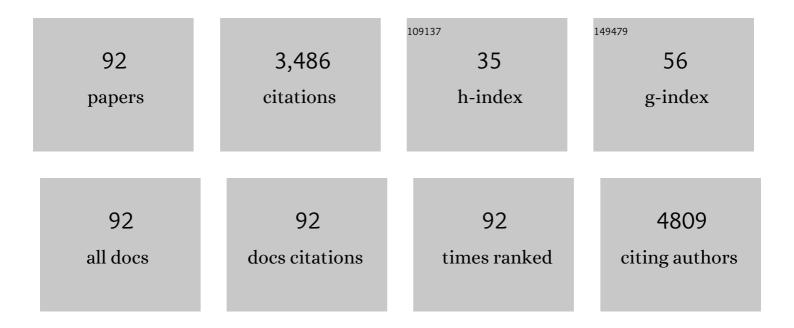
Seong-Hyeon Hong

List of Publications by Year in descending order

Source: https://exaly.com/author-pdf/1605019/publications.pdf Version: 2024-02-01



#	Article	IF	CITATIONS
1	Scalable synthesis of silicon nanosheets from sand as an anode for Li-ion batteries. Nanoscale, 2014, 6, 4297.	2.8	149
2	SnO2@Co3O4 hollow nano-spheres for a Li-ion battery anode with extraordinary performance. Nano Research, 2014, 7, 1128-1136.	5.8	123
3	Gas sensing properties of MoO3 nanoparticles synthesized by solvothermal method. Journal of Nanoparticle Research, 2010, 12, 1889-1896.	0.8	114
4	New Insight into Microstructure Engineering of Niâ€Rich Layered Oxide Cathode for High Performance Lithium Ion Batteries. Advanced Functional Materials, 2021, 31, 2010095.	7.8	113
5	Synthesis of SnO2 nano hollow spheres and their size effects in lithium ion battery anode application. Journal of Power Sources, 2013, 225, 108-112.	4.0	110
6	Anisotropic Grain Growth in Diphasicâ€Gelâ€Đerived Titaniaâ€Doped Mullite. Journal of the American Ceramic Society, 1998, 81, 1269-1277.	1.9	97
7	Calcium Phosphate Bioceramics with Various Porosities and Dissolution Rates. Journal of the American Ceramic Society, 2002, 85, 3129-3131.	1.9	96
8	Influence of Minor Ions on the Stability and Hydration Rates of βâ€Đicalcium Silicate. Journal of the American Ceramic Society, 2004, 87, 900-905.	1.9	92
9	Spark Plasma Sintering (SPS) of NASICON Ceramics. Journal of the American Ceramic Society, 2004, 87, 305-307.	1.9	88
10	Spark Plasma Sintering of LiTi2(PO4)3-Based Solid Electrolytes. Journal of the American Ceramic Society, 2005, 88, 1803-1807.	1.9	86
11	Sn ₄ P ₃ –C nanospheres as high capacitive and ultra-stable anodes for sodium ion batteries. Journal of Materials Chemistry A, 2018, 6, 17437-17443.	5.2	82
12	A nanopore-embedded graphitic carbon shell on silicon anode for high performance lithium ion batteries. Journal of Materials Chemistry A, 2018, 6, 8013-8020.	5.2	81
13	Anisotropic Abnormal Grain Growth in TiO ₂ /SiO ₂ â€Doped Alumina. Journal of the American Ceramic Society, 2000, 83, 2809-2812.	1.9	77
14	Stable Silicon Anode for Lithium-Ion Batteries through Covalent Bond Formation with a Binder via Esterification. ACS Applied Materials & Interfaces, 2019, 11, 26753-26763.	4.0	75
15	Substantially improved room temperature NO ₂ sensing in 2-dimensional SnS ₂ nanoflowers enabled by visible light illumination. Journal of Materials Chemistry A, 2021, 9, 11168-11178.	5.2	75
16	Revisiting Primary Particles in Layered Lithium Transitionâ€Metal Oxides and Their Impact on Structural Degradation. Advanced Science, 2019, 6, 1800843.	5.6	68
17	Electric and Dielectric Properties of Nb-Doped CaCu3Ti4O12Ceramics. Journal of the American Ceramic Society, 2007, 90, 2118-2121.	1.9	67
18	Meso-porous silicon-coated carbon nanotube as an anode for lithium-ion battery. Nano Research, 2016, 9, 2174-2181	5.8	67

#	Article	IF	CITATIONS
19	Effect of Liquid Content on the Abnormal Grain Growth of Alumina. Journal of the American Ceramic Society, 2001, 84, 1597-1600.	1.9	65
20	An approach to flexible Na-ion batteries with exceptional rate capability and long lifespan using Na ₂ FeP ₂ O ₇ nanoparticles on porous carbon cloth. Journal of Materials Chemistry A, 2017, 5, 5502-5510.	5.2	64
21	The Role of Zr Doping in Stabilizing Li[Ni _{0.6} Co _{0.2} Mn _{0.2}]O ₂ as a Cathode Material for Lithiumâ€lon Batteries. ChemSusChem, 2019, 12, 2439-2446.	3.6	61
22	Mullite Transformation Kinetics in P ₂ O ₅ â€, TiO ₂ â€, and B ₂ O ₃ â€Doped Aluminosilicate Gels. Journal of the American Ceramic Society, 1997, 80, 1551-1559.	1.9	59
23	H2 and C2H5OH sensing characteristics of mesoporous p-type CuO films prepared via a novel precursor-based ink solution route. Sensors and Actuators B: Chemical, 2013, 178, 395-403.	4.0	58
24	CuBi ₂ O ₄ Prepared by the Polymerized Complex Method for Gas-Sensing Applications. ACS Applied Materials & amp; Interfaces, 2018, 10, 14901-14913.	4.0	57
25	Revisiting the role of Zr doping in Ni-rich layered cathodes for lithium-ion batteries. Journal of Materials Chemistry A, 2021, 9, 17415-17424.	5.2	56
26	Effect of the Liquidâ€Forming Additive Content on the Kinetics of Abnormal Grain Growth in Alumina. Journal of the American Ceramic Society, 2003, 86, 1421-1423.	1.9	54
27	Effect of the Amine Concentration on Phase Evolution and Densification in Printed Films Using Cu(II) Complex Ink. Langmuir, 2015, 31, 8101-8110.	1.6	54
28	Challenges and recent progress in LiNixCoyMn1â^'xâ^'yO2 (NCM) cathodes for lithium ion batteries. Journal of the Korean Ceramic Society, 2021, 58, 1-27.	1.1	49
29	Highly stable SnO ₂ –Fe ₂ O ₃ –C hollow spheres for reversible lithium storage with extremely long cycle life. Nanoscale, 2018, 10, 4370-4376.	2.8	46
30	p-Type aliovalent Li(I) or Fe(III)-doped CuO hollow spheres self-organized by cationic complex ink printing: Structural and gas sensing characteristics. Sensors and Actuators B: Chemical, 2017, 243, 262-270.	4.0	44
31	Synthetic Mechanism Discovery of Monophase Cuprous Oxide for Record High Photoelectrochemical Conversion of CO ₂ to Methanol in Water. ACS Nano, 2018, 12, 8187-8196.	7.3	44
32	Apatite Induction on Ca-Containing Titania Formed by Micro-Arc Oxidation. Journal of the American Ceramic Society, 2005, 88, 2642-2644.	1.9	42
33	Direct Printing Synthesis of Self-Organized Copper Oxide Hollow Spheres on a Substrate Using Copper(II) Complex Ink: Gas Sensing and Photoelectrochemical Properties. Langmuir, 2014, 30, 700-709.	1.6	41
34	Coarsening Behavior of Tricalcium Silicate (C ₃ S) and Dicalcium Silicate (C ₂ S) Grains Dispersed in a Clinker Melt. Journal of the American Ceramic Society, 2000, 83, 1247-1252.	1.9	40
35	Effect of Al Doping on the Electric and Dielectric Properties of CaCu ₃ Ti ₄ O ₁₂ . Journal of the American Ceramic Society, 2007, 90, 4009-4011.	1.9	38
36	Fabrication of Ga ₂ O ₃ /SnO ₂ core–shell nanowires and their ethanol gas sensing properties. Journal of Materials Research, 2011, 26, 2322-2327.	1.2	36

#	Article	IF	CITATIONS
37	Stepwise Dopant Selection Process for Highâ€Nickel Layered Oxide Cathodes. Advanced Energy Materials, 2022, 12, .	10.2	35
38	p-Type CuBi 2 O 4 thin films prepared by flux-mediated one-pot solution process with improved structural and photoelectrochemical characteristics. Materials Letters, 2017, 188, 192-196.	1.3	34
39	Manganese Tetraphosphide (MnP ₄) as a High Capacity Anode for Lithiumâ€lon and Sodiumâ€lon Batteries. Advanced Energy Materials, 2021, 11, 2003609.	10.2	34
40	Characterization of Ca ₂ SiO ₄ :Eu ²⁺ Phosphors Synthesized by Polymeric Precursor Process. Journal of the American Ceramic Society, 2009, 92, 2025-2028.	1.9	33
41	Fabrication of Silicon Nitride Nanoceramics and their Tribological Properties. Journal of the American Ceramic Society, 2010, 93, 1461-1466.	1.9	33
42	Reversible storage of Li-ion in nano-Si/SnO2 core–shell nanostructured electrode. Journal of Materials Chemistry A, 2013, 1, 3733.	5.2	33
43	Synthesis and Photoluminescence Properties of Eu3+-Doped Calcium Phosphates. Journal of the American Ceramic Society, 2007, 90, 2795-2798.	1.9	32
44	Photoluminescence Characteristics of Sr3SiO5:Eu2+ Yellow Phosphors Synthesized by Solid-State Method and Pechini Process. Journal of the Electrochemical Society, 2011, 158, J330.	1.3	32
45	Microscopic Evidence for Strong Interaction between Pd and Graphene Oxide that Results in Metalâ€Decorationâ€Induced Reduction of Graphene Oxide. Advanced Materials, 2017, 29, 1605929.	11.1	32
46	Dielectric and magnetic properties in Ta-substituted BiFeO ₃ ceramics. Journal of Materials Research, 2007, 22, 3397-3403.	1.2	31
47	<i>An in situ</i> formed graphene oxide–polyacrylic acid composite cage on silicon microparticles for lithium ion batteries <i>via</i> an esterification reaction. Journal of Materials Chemistry A, 2019, 7, 12763-12772.	5.2	31
48	Uniform Coating of Nanometer-Scale BaTiO3 Layer on Spherical Ni Particles via Hydrothermal Conversion of Ti-Hydroxide. Journal of the American Ceramic Society, 2005, 88, 303-307.	1.9	29
49	CO gas sensing properties in Pd-added ZnO sensors. Journal of Electroceramics, 2009, 23, 196-199.	0.8	29
50	Superior sodium storage performance of reduced graphene oxide-supported Na _{3.12} Fe _{2.44} (P ₂ O ₇) ₂ /C nanocomposites. Chemical Communications, 2017, 53, 9316-9319.	2.2	25
51	Photoelectrochemical hydrogen production at neutral pH phosphate buffer solution using TiO2 passivated InAs Nanowire/p-Si heterostructure photocathode. Chemical Engineering Journal, 2020, 392, 123688.	6.6	23
52	Enhanced Lithium Storage in Reduced Graphene Oxide-supported M-phase Vanadium(IV) Dioxide Nanoparticles. Scientific Reports, 2016, 6, 30202.	1.6	22
53	V4P7@C nanocomposite as a high performance anode material for lithium-ion batteries. Journal of Power Sources, 2018, 400, 204-211.	4.0	22
54	A P2-type Na _{0.7} (Ni _{0.6} Co _{0.2} Mn _{0.2})O ₂ cathode with excellent cyclability and rate capability for sodium ion batteries. Chemical Communications, 2019, 55, 11575-11578.	2.2	22

#	Article	IF	CITATIONS
55	Alternative Explanation for the Role of Magnesia in the Sintering of Alumina Containing Small Amounts of a Liquid Phase. Journal of the American Ceramic Society, 2003, 86, 634-39.	1.9	21
56	Coating of TiO2 nanolayer on spherical Ni particles using a novel sol-gel route. Journal of Materials Research, 2004, 19, 1669-1675.	1.2	20
57	Blueâ€emitting AlN:Eu ²⁺ Powder Phosphor Prepared by Spark Plasma Sintering. Journal of the American Ceramic Society, 2010, 93, 356-358.	1.9	20
58	Tribological Properties of <scp><scp>Si₃N₄</scp></scp> <scp>SiC</scp> Nano–Nano Composite Ceramics. Journal of the American Ceramic Society, 2011, 94, 3683-3685.	1.9	20
59	Effect of Surface Impurities on the Microstructure Development during Sintering of Alumina. Journal of the American Ceramic Society, 2001, 84, 1386-1388.	1.9	19
60	TiO2@SnO2@TiO2 triple-shell nanotube anode for high-performance lithium-ion batteries. Journal of Solid State Electrochemistry, 2017, 21, 2365-2371.	1.2	17
61	Electrical Transport and Thermoelectric Properties of SnSe–SnTe Solid Solution. Materials, 2019, 12, 3854.	1.3	17
62	Mesoporous Nanoâ€ s i Anode for Liâ€ion Batteries Produced by Magnesioâ€Mechanochemical Reduction of Amorphous SiO ₂ . Energy Technology, 2013, 1, 327-331.	1.8	16
63	Effect of ultra-thin SnO2 coating on Pt catalyst for energy applications. International Journal of Precision Engineering and Manufacturing, 2016, 17, 691-694.	1.1	16
64	A MnV ₂ O ₆ /graphene nanocomposite as an efficient electrocatalyst for the oxygen evolution reaction. Nanoscale, 2020, 12, 16028-16033.	2.8	16
65	Tunable conductivity at LaAlO3/SrxCa1â^'xTiO3 (0 â‰≇€‰x â‰≇€‰1) heterointerfaces. Applied Phy 102, 012903.	sics Letters	s, 2 <u>0</u> 13,
66	Synthesis and hydration behavior of calcium zirconium aluminate (Ca7ZrAl6O18) cement. Cement and Concrete Research, 2014, 56, 106-111.	4.6	14
67	Solid solution phosphide (Mn _{1â^'x} Fe _x P) as a tunable conversion/alloying hybrid anode for lithium-ion batteries. Nanoscale, 2019, 11, 13494-13501.	2.8	14
68	Visible Light Driven Ultrasensitive and Selective NO ₂ Detection in Tin Oxide Nanoparticles with Sulfur Doping Assisted by <scp>l</scp> ysteine. Small, 2022, 18, e2106613.	5.2	14
69	Superior electrochemical sodium storage of V ₄ P ₇ nanoparticles as an anode for rechargeable sodium-ion batteries. Chemical Communications, 2019, 55, 3207-3210.	2.2	13
70	Electrochemical Properties and Reaction Mechanism of NiTi ₂ S ₄ Ternary Metal Sulfide as an Anode for Lithium Ion Battery. ACS Sustainable Chemistry and Engineering, 2021, 9, 9680-9688.	3.2	13
71	Mesoporous Si–Cu nanocomposite anode for a lithium ion battery produced by magnesiothermic reduction and electroless deposition. Nanotechnology, 2019, 30, 405401.	1.3	12
72	Preparation of SnO2 whiskers via the decomposition of tin oxalate. Journal of Electroceramics, 2006, 17, 895-898.	0.8	11

#	Article	IF	CITATIONS
73	Nanoscale ZnO and Alâ€Doped ZnO Coatings on ZnS:Ag Phosphors and their Cathodoluminescent Properties. Journal of the American Ceramic Society, 2008, 91, 451-455.	1.9	11
74	Texture Evolution of Abnormal Grains with Post-Deposition Annealing Temperature in Nanocrystalline Cu Thin Films. Metallurgical and Materials Transactions A: Physical Metallurgy and Materials Science, 2013, 44, 152-162.	1.1	11
75	Giant Electroresistive Ferroelectric Diode on 2DEG. Scientific Reports, 2015, 5, 10548.	1.6	10
76	Lateral epitaxial growth of faceted SnO ₂ nanowires with self-alignment. CrystEngComm, 2014, 16, 9340-9344.	1.3	8
77	Synthesis and Hydration Characteristics of Alinite Cement. Journal of the American Ceramic Society, 2002, 85, 1941-1946.	1.9	7
78	Novel Calcium Zirconate Silicate Cement Biomineralize and Seal Root Canals. Materials, 2018, 11, 588.	1.3	7
79	NiP2/C nanocomposite as a high performance anode for sodium ion batteries. Electrochimica Acta, 2022, 403, 139686.	2.6	7
80	Synthesis of well-aligned SnO2 nanowires with branches on r-cut sapphire substrate. CrystEngComm, 2012, 14, 1545.	1.3	6
81	A Novel Solid Solution Mn1-xVxP Anode with Tunable Alloying/Insertion Hybrid Electrochemical Reaction for High Performance Lithium Ion Batteries. Energy Storage Materials, 2021, 41, 310-320.	9.5	6
82	Interfacial precipitation in titania-doped diphasic mullite gels. Journal of Materials Research, 1998, 13, 974-978.	1.2	5
83	Hydration behavior and radiopacity of strontium substituted Ca3SiO5 cement. Journal of the Korean Ceramic Society, 2021, 58, 330-336.	1.1	4
84	Effect of Co-Precipitation on the Low-Temperature Sintering of Biphasic Calcium Phosphate. Journal of the American Ceramic Society, 2006, 89, 060427083300032-???.	1.9	3
85	Hetero-epitaxial growth of vertically-aligned TiO2 nanorods on an m-cut sapphire substrate with an (001) SnO2 buffer layer. CrystEngComm, 2012, 14, 4963.	1.3	3
86	Epitaxial recrystallization and luminescence of CaAl2O4:Eu2+ thin films prepared on sapphire substrates. Journal of Electroceramics, 2013, 30, 36-40.	0.8	3
87	Microstructure Modification of Liquid Phase Sintered Fe–Ni–B–C Alloys for Improved Mechanical Properties. Metallurgical and Materials Transactions A: Physical Metallurgy and Materials Science, 2021, 52, 4395-4401.	1.1	3
88	Kinetic stabilization of a topotactically transformed texture morphology <i>via</i> doping in Ni-rich lithium layered oxides. Journal of Materials Chemistry A, 2022, 10, 13735-13743.	5.2	3
89	Graphene Oxide: Microscopic Evidence for Strong Interaction between Pd and Graphene Oxide that Results in Metalâ€Decorationâ€Induced Reduction of Graphene Oxide (Adv. Mater. 15/2017). Advanced Materials, 2017, 29, .	11.1	1
90	Mapping the electrocatalytic water splitting activity of VO ₂ across its insulator-to-metal phase transition. Nanoscale, 2022, 14, 8281-8290.	2.8	1

#	Article	IF	CITATIONS
91	Characteristics of Liquid Penetration into Undoped and Magnesiaâ€Doped Alumina. Journal of the American Ceramic Society, 2003, 86, 2206-2208.	1.9	0
92	Effects of sintering conditions on the microstructure and mechanical properties of SiC prepared using powders recovered from kerf loss sludge. Bulletin of Materials Science, 2018, 41, 1.	0.8	0